Recent, rapid restructuring of North American bumble bee communities is associated with climate warming

Jeremy Hemberger[1] *, Neal Williams[1]

[1] Department of Entomology and Nematology, University of California Davis. One Shields Ave, Davis, CA 95616 USA

* Corresponding author address: Department of Entomology, University of Wisconsin-Madison. 1630 Linden Dr, Madison, WI 53706

Phone: (608) 622-2698

Email address: j.a.hemberg@gmail.com

Abstract

A rapidly warming climate has become one of the primary forces driving changes in biodiversity worldwide. The impact of warming temperatures on insect communities is of particular interest given their importance for ecosystem function and service provision and the uncertainty around whether insect communities can keep pace with the rate of increasing temperatures. We use a long-term dataset on bumble bee species occurrence and data on summer maximum temperature trends across North America to characterize community-level responses to recent climate warming. Bumble bees are relatively well recorded historically and are sensitive to warming temperatures. We examined responses using the community temperature index (CTI) – a measure of the balance of cool- and warm-adapted species within local communities. Starting in 2010, bumble bee average CTI across North America has rapidly increased after a period of slight increase from 1989 to the late 2000s. This increase is strongly associated with recent increases in maximum summer temperatures. The increase in CTI is spatially extensive, occurring throughout North America, but the areas of greatest concern include mid to high latitudes as well as low and high elevations - areas relatively shielded from other intensive global changes (e.g., land-use). On average, bumble bee CTI has increased 0.99°C from 1989 to 2018, a change of similar magnitude to the increase in maximum summer temperatures. The rapid shift in bumble bee communities appears to be at pace with shifting summer temperatures, with an approximate, equivalent northward shift of ~104 km from 1989-2018 for both. This indicates an adaptive capacity among some bumble bee species. However, warming temperatures are also likely reducing the occurrence and local abundance of cool-adapted species that may serve important ecological roles within their range. Our results provide strong evidence of the pervasive impacts posed to insect communities by temperature increases in the past few decades.

Introduction

Climate change is driving profound changes in animal occurrence and community composition worldwide. Long-term increases in average temperature as well as increases in acute, extreme weather events (e.g., heat waves) have been linked to both positive [CITE] and negative outcomes for biodiversity [CITE]. Regardless of the direction of such outcomes, a rapidly changing climate has the potential to fundamentally alter biological processes, including ecosystem services that maintain biodiversity and support global agricultural production [CITE].

Insect responses to climate change are of specific interest given the growing documentation of declines in a variety of taxa and regions [CITE]. Although several anthropogenic drivers of global change are at play [@Hemberger.2021, MORE], a changing climate is particularly menacing given the number of potential direct and indirect impacts it has on insects and its capacity to be a force-multiplier, interacting with other factors to exacerbate changes in insect populations [CITE]. Like many global change drivers, rapidly increasing temperatures may favor some species while leading to local extirpations of others. Though critical limits of species [e.g., CT_{max}. Oyen.2018] are unlikely to be breached, the extent to which climate warming has contributed to local shifts in insect abundance and species' range remains unknown - placing a host of ecological processes and services in limbo.

Even among the most studied insect taxa there is debate about the extent, severity, and direction of effects associated with climate change. Bumble bees are a prime example with some studies revealing extensive declines [@Soroye.2020; but see @Guzman.2021] and others suggesting resilience and relative stability [@Maebe.2021; @Guzman.2021] or mixed patterns of decline and increases over time[@Jackson.2022]. Most current approaches examining the long-term influence of climate on bumble bees use occupancy models to relate changes in species occurrence to trends in climate, such as increases in temperature and changes in precipitation [@Januosek.2023]. Although this method can yield valuable insights, it can be challenging to align the framework with the incidental and imperfect occurrence data that abounds in large-scale insect databases, making model outcomes sensitive to occupancy assumptions [@Guzman.2021]. Moreover, the occupancy approach framework does not capture the physiological mechanisms driving species responses to warming temperatures. As such, a more thorough understanding of where/when insects are most impacted by climate change requires exploring alternative analytical methods that better tie climatic changes to estimates of insect physiological preferences and limits.

We characterize bumble bee community responses to recent climate warming at the continental scale by examining changes in the community temperature index (CTI), a physiological metric of community responses to climate based on the composition of cool- and warm-adapted species. This metric can be used to assess the rate of change in community composition based on historical species temperature preferences (species temperature index, STI), as well as the spatial velocity of community changes [@Devictor.2008; @Devictor.2012]. When examined over time along with temperature, CTI can help determine whether species are keeping pace with the velocity of temperature

trends [i.e., an increase in warm-adapted species and a loss of cool-adapted species in rapidly warming areas; @Fourcade.2019], or whether communities are accruing "climate debts", as rising temperatures outpace species turnover [@Devictor.2012]. ~~This method also simultaneously assesses changes at the edge of species' ranges (i.e., colonization/extirpation) and those in the core (i.e., increases in abundance).~~

Using 50 years of records from the Bumble bees of North America database (Richardson 202X), we test for changes in bumble bee communities using CTI across North America and quantify CTI shifts' association with trends in maximum summer temperatures. Specifically, we wanted to address the following questions: (1) is there evidence of an increase in bumble bee CTI over time? (2) are changes in CTI associated with increases in summer temperatures? (3) are CTI changes greater in areas particularly vulnerable to a changing climate (e.g., higher latitudes and elevations)? (4) are the observed shifts in CTI keeping pace with the rate of temperature increases (i.e., are communities accruing "climate debt") and (5) which species are driving any observed changes in CTI? We predicted a steady increase in bumble bee CTI in accordance with documented increases in average maximum summer temperatures over the past century and that changes would be more dramatic at higher latitudes and elevations. We also expected that a host of common species that have increased in occurrence over the past several decades would be the strongest drivers of change in CTI across the continent.

Methods

North American bumble bee occurrence and community data

We used occurrence records for 59 species of North American bumble bees from the bumble bees of North America database [BBNA; @Richardson.2022]. This database composes 781,280 records from 1805-2020 from a variety of sources (e.g., natural history collections, research studies, citizen science programs). Because the database consists of an amalgam of sources, we took several steps to account for known biases [@Bartomeus.2019; @Gotelli.2021]. The species and community temperature indices at large scales of our analysis are robust to imprecision in the underlying distributional data [@Devictor.2008]; nonetheless we filtered the original dataset to include only complete records (i.e., identified to species, containing complete coordinates) and unique collection events (distinct combinations of species, date, coordinates, and observer; Figure S1A). This step helps to minimize the bias associated with unequal sampling efforts and differential data collection methods across all observers. Moreover, we conducted a range of sensitivity analyses (see below) to determine whether our results were robust given our assumptions and methodological decisions.

Is there evidence of an increase in bumble bee CTI over time?

Calculating the CTI first requires the species temperature index (STI; i.e., the historical average summertime temperature experienced over a species' approximate range; Figure S1B) to be calculated. We used a subset of occurrence records from 1970-2000 to extract historical summertime temperature associations and calculate the STI for each species. In this, we assumed that the records contained within this period are representative of the entire range of each species. Using the `raster` package [@raster], we extracted temperatures at the specific location (i.e., raster pixel) of each occurrence record from the raster of average historical maximum summer temperatures using WorldClim version 2.1 historical climate data for maximum monthly temperatures at 30 arc-second (~1 km^2) resolution [@Fick.2017]. To create a raster of historical maximum summer temperatures, we calculated the average maximum monthly temperature for summer months (defined here as June-September) for a historical period of 1970 to 2000. We then used this raster to extract STI values using our bumble bee occurrence records.

Our analysis framework required us to assign records to communities to calculate CTI for given locations/times (Figure S1C. Although the species assemblages we define below are considerably larger than the scale of an ecological community, the analysis is ultimately agnostic to this point, and it does not affect our specific questions. We refer to them as communities/CTI to maintain consistency with the existing literature. Also, because we used occurrence records from a variety of sources whose spatial locations varied over time, using fixed sampling locations was not possible. Instead, we created a hexagonal grid across North America at a broad spatial scale (50 km hexagonal grid resolution, center to side: ~ 6600 km^2) to act as stand-in "community" boundaries. We chose a 50 km resolution to ensure we would capture sufficient records within each grid cell to robustly estimate the broad spatiotemporal trend of CTI [Jackson.2021]. To determine if the resolution of our grid cells impacted our results, we also conducted our analyses using 10 and 100 km

center-to-side hexagonal grid cells. We assigned bumble bee occurrence records to each grid cell to create quasi-communities, requiring each cell to contain at least 2 species for a given year to calculate CTI. We used hexagonal grid cells to minimize possible edge effects and provide a better fit across the curvature of the earth at large spatial scales [e.g., continental; @Birch.2007].

Using STI values, we then calculated CTI within each grid cell where at least 2 species records were present in the grid using the full set of bumble bee occurrence records from 1961-2018 (Figure S1D. We calculated CTI using two different methods, first using occurrence records for species *i* occurring within a given community (grid cell) *j*

$$Equation\ 1: Occurrence\ CTI_j = \frac{\sum_{i=1}^{n} STI_{i,j}}{n}$$

and then using abundance weighted estimates of species within each community:

$$Equation\ 2: Abundance\ weighted\ CTI_j = \frac{\sum_{i=1}^{n} a_{i,j} \times STI_{i,j}}{\sum_{i=1}^{n} a_{i,j}}$$

where $a_{i,j}$ is the abundance of species *i* at site *j,* and *n* is the total number of species within a grid cell [@Prince.2014]. These two approaches, though similar, estimate the two mechanisms of change in CTI. Using occurrence records (Equation 1) allowed us to test shifts in CTI due to changes in occurrence (i.e., immigration/extirpation), while calculating CTI using abundance weighting (Equation 2) allowed us to understand shifts in CTI as a function of changes in local relative abundance (i.e., species becoming more common/rare within a given community).

Are changes in CTI associated with increases in summer temperatures?

To determine long-term warming trends across North America, we used WorldClim gridded historical monthly weather data from 1961-2018 for our defined summer months [@Fick.2017]. First, we averaged the maximum monthly temperature for each year. Second, we extracted the mean maximum temperature within each of the bumble bee community grid cells (Figure S1E). This procedure created a time series of the average maximum summer temperature for each year/grid cell from 1961-2018. Third, we calculated the average maximum summer temperature for a historical period from 1961-2000 for each grid cell; this is our baseline and we refer to it as the temperature "normal". Last, we calculated the summer maximum temperature anomaly (defined here as the deviation from long-term normal) and averaged these using 3 moving-window scales of 3, 10, and 30 years to capture metrics of relatively short- , medium-, and long-term changes in maximum summer temperatures, respectively. To illustrate the estimated trends in maximum summertime temperatures, we calculated the change in our 3 scales of anomalies by subtracting the 1990 anomaly (first year possible to calculate 30-year average) from the 2018 anomaly for each grid cell.

We used generalized additive models (GAM) to quantify trends in CTI over space and time and determine whether changes in CTI were related to short-, medium-, and long-term trends in temperature anomalies (Figure S1F). Generalized additive models provide a highly flexible computational framework to account for variable trends in spatiotemporal

processes [@Pedersen.2019] and are especially well-suited for the analysis of potentially complex time series and can readily identify periods of significant change [@Simpson.2018].

For each measure of CTI (occurrence and abundance-weighted), we fitted a GAM to model the effects of spatial location (latitude, longitude, and elevation), long-term trend (year), short-, medium-, and long-term estimates of rising temperatures (3, 10, and 30-year summertime maximum temperature anomalies). For the remainder of this manuscript, we refer to this GAM as the global model.

$$Equation\ 3\text{: } CTI_j \sim s(lat, long) + s(year) + s(elevation) + ti(lat, long, year, elevation) + s(eco\ region, bs = \text{"re"}) + \text{s}(\bar{T}_{\max 3}) + \text{s}(\bar{T}_{\max 10}) + \text{s}(\bar{T}_{\max 30})$$

We fit the model using the `mgcv` package in R [@mgcv]. The goal of each model was to identify any temporal trends in CTI and determine where and when significant changes have occurred. Because of the differences in geography, land-use, and climate across North America, we included a 2-dimensional smooth of latitude and longitude, and we allowed the estimated temporal trend in CTI to vary according to spatial location by including a tensor product interaction of latitude, longitude, elevation, and year (Equation 3). We also included a random effect smooth of ecological region (level 1) to further account for variation in the response of CTI in accordance with common biophysical characteristics within ecological regions, such as commonalities in vegetation and other climate variables (e.g., precipitation). We included smooths of 3-, 10-, and 30-year summertime maximum temperature anomalies to determine whether changes in CTI were correlated with trends in warming maximum summer temperatures. Including three different anomaly scales allowed us to assess the temporal scale of temperature change bumble bee communities respond most strongly to. This model was fit to CTI estimates from 1989-2018 because 1989 was the first year for which 30-year temperature anomalies could be calculated. We tested the model for spatial and temporal autocorrelation in the residuals. For spatial autocorrelation, we tested simulated residuals with a Moran's I test using the `dHARMA` package [@dharma]. For temporal autocorrelation, we visually examined the autocorrelation function using scaled, simulated residuals.

To visualize the change in CTI over time, we generated CTI predictions across the spatial and temporal extents of our dataset using the global model for each grid cell. We then determined the change in CTI from 1989-2018 by subtracting the CTI estimate for 1990 from that of 2018 for each grid cell. To visualize model uncertainty, we calculated the average standard error of global model predictions for each grid cell from 1990-2018. We visualized the effect of the three moving-average temperature anomalies on CTI by plotting the partial effects (prediction of CTI as a function of temperature holding other variables are at their mean value) of each anomaly from the global model using the `gratia` [@gratia] package.

Are CTI changes greater in areas particularly vulnerable to a changing climate (e.g., higher latitudes and elevations)?

To determine whether CTI changes were most drastic (i.e., greater slope in fitted GAM) in areas known to be experiencing accelerated climatic changes, we examined the rate of

change in the slope (i.e., first derivative) of our fitted model smooth (Fig. S2). To do this, we first fitted a GAM to CTI predictions with a single smooth of year to create a spatially explicit, estimated trend of CTI for each grid cell. Then, for each grid cell's fitted GAM year smooth, we extracted the first derivative with respect to time (1990-2018) using the `derivatives()` function from the `gratia` package [@gratia]. For elevation and latitude, we calculated the mean derivative value for each grid cell (i.e., the average rate of change of the CTI of a grid cell from 1989-2018) and then plotted this against the mean elevation and latitude of the grid cell. We visualized the relationship with a GAM fit using the `geom_smooth()` function in the ggplot [@tidy] package. To determine whether CTI changes were consistent or have accelerated over time, we calculated the derivative values for the year smooth for each grid cell and plotted these values against the year. Like elevation, this relationship was visualized with a simple GAM fit.

Are the observed shifts in CTI keeping pace with the rate of temperature increases (i.e., are communities accruing "climate debt")

By calculating the ratio of the temporal rate of change in CTI (i.e., how much is CTI changing per year) with that of the spatial rate of change (i.e., how much is CTI changing per degree of latitude), we can approximate the velocity of the northward shift for bumble bee communities ($°C\ yr^{-1}/°C\ km^{-1} = km\ yr^{-1}$). This metric provides an approximation of how much communities have effectively shifted northward in terms of their composition (Devictor et al., 2008, 2012) A similar procedure can be performed to calculate the spatial velocity in temperature. We estimated the rates of change for CTI over time by calculating the average derivative value of the "year" smooth in the model. For the spatial trend, we fit a GAM to the model predictions of CTI and related these to a single smooth of latitude and then calculated the average derivative value of the "latitude" smooth. We compared the approximate spatial velocities of CTI and temperature to determine whether there is a lag between the shifts in temperature and the communities' response. A lag would indicate that temperatures are increasing faster than communities are able to respond, thus accruing "climate debt".

Which species are driving any observed changes in CTI?

Although quantifying the trend in CTI provides evidence for whether communities are being restructured in response to a changing climate, the procedure does not implicitly identify which species are responsible for driving any observed increases. To address this, we used a jackknife analysis [@Prince.2014], iteratively eliminating one species from our model dataset and refitting the global model. For this analysis, we filtered to the grid cells that were within the range of the given species. The range was determined by creating a convex hull around all species occurrence records used in STI calculations and extracting the grid cells within this estimated range. To determine whether a species contributed to the trend in CTI, we fit a GAM with a single smooth of year to the predicted CTI values of grid cells within a species' range and then calculated the percent difference between the mean first derivative of the fitted year smooth in the reduced model predictions to that of the global model predictions. In this context, a positive percentage change indicated that a species had a positive contribution toward the CTI trend (i.e., the average slope of the year smooth increases when the species is included). That is, either more occurrences, or an

increase in the local abundance of this species leads to an increase in CTI. Conversely, species with a negative percent change had a negative contribution toward the CTI trend; as those species occur less frequently or decrease in local abundance, the CTI trend should increase.

Model validation

We performed cross validation on our global model using testing data that was filtered out of the full BBNA database. These collection events, while not "unique" (i.e., not necessarily fully independent given our strict definition), were still valid records that could be used to calculate the CTI for any given location. Upon calculating the CTI for grid cells using these records, we compared the values against predictions from the global model by using the coefficient of determination (R^2), root mean square error (RMSE) and mean absolute error (MAE).

Despite the vast number of individual occurrence records within our dataset, there were many grid cells that did not contain species occurrence data for fitting the model. Given that we explicitly model CTI over space, we presented our results above using predictions within all grid cells given the strength of our global model fits. However, we also assessed the results when using model predicted values of CTI only for grid cells containing occurrence data. This approach was primarily meant to provide conservative estimates of CTI changes, particularly where in space (i.e., latitude, elevation) and time changes were greatest.

We conducted all data wrangling, GIS operations, modeling, and visualization using R [@rcite] using the aforementioned and following packages: `tidyverse` [@tidy], `raster` [@raster], `sf` [@sf], `performance` [@performance], `janitor` [@janitor], `paletteer` [@paletteer], exactextractr [@exactextract], `foreach` [@foreach], and `data.table` [@datatable] packages.

Results

Bumble bee community temperature index has increased across a majority of North America

From 1989-2018 bumble bee CTI increased substantially across most of North America, but the magnitude of change was spatially variable - with an overall average increase of 0.99 ± 1.98 °C (mean ± SD) and a range of a decrease of 6.30 °C to an increase of 7.99 °C (Fig. 1A). The predictions were most certain across the coterminous United States where there is a high density of bumble bee records and less certain in the most northern grid cells of our study region in the high Tundra and Queen Elizabeth Islands as well as in the tropical wet forests of Mexico (Fig. 1B). The spatial trends of the increase in CTI were nearly identical between occurrence and abundance-weighted CTI; however, changes in occurrence CTI were marginally smaller (0.78 ± 1.75 °C). The global model, which quantified the change in CTI as a function of space, time, and changes in short-, medium-, and long-term temperature increases, explained a substantial portion of the deviance in both the abundance-weighted (Table S1; 86.0%, adj-R^2 = 0.849) and occurrence models (Table S1; 86.3%, adj-R^2 = 0.851).

The results of our analysis were consistent irrespective of the grid scale used in aggregating communities (Fig. S3; Table S2). The exception was in areas of British Columbia and Alaska where a highly concentrated spatial pattern of bumble bee records likely led to a predicted decrease in CTI in grid cells when aggregated at the 50 and 25 km grid scale. Aggregating at the largest scale (100 km center-to-side hexagonal grid) revealed the most wide-spread increases in CTI, with nearly all grid cells exhibiting an increase in CTI from 1989 to 2018.

Our models performed well when cross-validated using withheld data from the BBNA database (Fig. S4). Coefficient of determination (R^2) values ranged from 0.79-0.81, root mean squared error (RMSE) ranged from 1.22-1.31, and mean absolute error (MAE) ranged from 0.91-0.96. In addition, our model performance was consistent across the three tested grid scales. Predictions were most accurate for CTI values ranging from 23-28°C which corresponded to the regions where the bulk of the occurrence records were collected. Prediction accuracy was most variable among cool regions in the north and sub-arctic (CTI < 23°C).

Shifts in CTI are strongly related to long-term increases in summer temperature

Summertime maximum temperatures have increased by 1989-2018 (Fig. 1C-E), with increases most apparent at 10- (0.630 ± 0.405 °C) and 30-year average anomalies (0.969 ± 0.342°C; Fig. 1D, E; Fig. S5). Increases in the 30-year summertime maximum temperature anomaly showed a strong statistical association with increases in bumble bee CTI (Fig. 2C; F = 4.561, p = 0.002). Increases in the 30-year temperature anomaly between 0-0.5°C had no impact on CTI. However, increases beyond 0.5°C were associated with a rapid increase of up to 1°C in bumble bee CTI (partial effect due solely to 30-year temperature anomaly). Of the 2,425 grid cells, 1,753 exhibited parallel increases in change in CTI and the change in the 30-year temperature anomaly between 1989-2018 (Fig. 3A). Beyond a 1°C change in the 30-year temperature anomaly the changes in CTI rapidly increase, with gains of 1 to

6.8°C. The relationship of CTI with short term, 3-year moving average shifts in summer temperature anomalies, while statistically supported, was weak and variable over the range of the anomalies (Fig. 2A; F = 2.584, p = 0.032). There was no statistically supported relationship between the 10-year average anomaly and bumble bee CTI (Fig. 2B; F = 0.064, p = 0.802).

CTI is increasing fastest at low and high elevations, latitudes, and more recent years

We examined patterns in the rate of change in CTI across the continent to determine where and when the most extreme changes in CTI were occurring and whether these areas overlapped with areas known to be heavily impacted by a warming climate [@Januosek.2023]. The rate of change in CTI was greatest at low (< 800 m) and high elevations (> 2000 m; Fig. 4A) and increased with increasing latitude (Fig. 4B). Moreover, the rate of change in CTI has increased from 1989-2018, with CTI increasing most rapidly after 2010 (Fig. 4C). These results varied slightly when analyzed with predictions from only grid cells containing occurrence records, with changes in CTI being greatest at high elevations (Fig. S6A; > 2000 m) and mid-high latitudes (Fig. S6B; 35 – 60°). The temporal patterns of the rate of change were largely similar but were positive only from 2003 and beyond (Fig. S6C), confirming the accelerating rate of CTI change from 2010 onward that is exhibited when using predictions from all grid cells (Fig. 4C).

Bumble bee community changes are keeping pace with climate warming

The spatial velocity of bumble bee CTI increases (3.58 km yr^{-1}) was nearly identical to that of summer temperature increases (3.59 km yr^{-1}). Over the course of the study (29 years), bumble bee communities and summer temperatures have exhibited an equivalent northward shift of approximately 104 km. This comparison, while highly dependent on the complexity of the GAM smooths used to estimate the spatial and temporal trends, indicates that shifts within bumble bee community composition are effectively keeping pace with the rate of climate warming.

Species contributions to changes in CTI

All but 3 species had positive contributions toward the mean derivative of the temporal trend in bumble bee CTI from 1989-2018 (Table S3). Of the most represented species in the dataset, *B. occidentalis* (% Δ = 70.42%), *B. nevadensis* (% Δ = 69.65%), *B. ephippiatus* (% Δ = 66.87%), *B. bifarius* (% Δ = 66.71%), and *B. vosnesenski*i (% Δ = 64.32%) had the greatest contribution for both abundance-weighted and occurrence CTI trends. Of the top 25 contributors to the increase in CTI, 14 (56%) are in the subgenus Pyrobombus (and 3 of the top 5). In general, species with wider ranges and more variable STI tended to be those that had the biggest contributions toward the long-term increase in CTI.

Discussion

We documented significant, spatially-extensive shifts in the thermal tolerance of species within North American bumble bee communities in response to long-term increases in summer temperatures. Over the last 29 years across the continent, bumble bee community assemblages increasingly consist of either more warm-adapted or fewer cold-adapted species, with increases in community temperature index, the measure of the balance of warm- and cool-adapted species, most pronounced at mid- to high latitudes, and high elevations in the American Rockies, Intermountain West, and central Mexico. The community temperature index increased according to both occurrence and abundance-weighted indices, suggesting that shifts in both local abundance and broader changes in species occurrence (i.e., range shifts) underlie the changes in community composition. The rapid shift in bumble bee communities appears to be on pace with shifting summer temperatures, with an approximate, equivalent northward shift of ~104 km from 1989-2018 for both CTI and temperature. Our work provides additional evidence of the pervasive impacts a warming planet has for insect biodiversity (CITE OTHER) and identifies regions of concern where anthropogenic climate warming is rapidly restructuring the communities of an ecologically important group of insects.

An increase of warm-adapted species within biological communities is a logical consequence of a rapidly warming climate [@Beissinger.2013]. Similar shifts have been observed in bird communities in response to both warming summer [@Devictor.2009; @Devictor.2012] and winter [@Prince.2014] temperatures. Because insects are ectotherms, temperature-induced shifts in range and abundance may be even more pronounced. Indeed, large changes in insect CTI have been observed for both bumble bees [@Fourcade.2018] and butterflies [@Devictor.2012]; however, trends in CTI are often not explicitly tied to spatial and temporal patterns of warming temperatures. Our results provide this link and show a clear statistical relationship between increases in CTI and long-term increases in maximum summer temperatures across North America, with areas experiencing a 30-year temperature anomaly of greater than or equal to 0.5°C strongly associated with a rapid increase in bumble bee CTI. These results identify areas of ample concern where rates of bumble bee community change and summer temperature increases are the greatest (Fig. 1; dark orange and red areas).

The frontline of species' responses to climate have tended to be at high latitudes and elevations. Northern regions have experienced rapid increases in temperature leading to pronounced phenological shifts across taxa [@Parmesan.2007]. Our results support this trend, finding greatest rates of bumble bee CTI change at higher latitudes and high elevation. The bumble bee species in these locations tend to have narrower ranges and be cold-adapted, traits identical to other insect taxa that have exhibited declines due to climate [@Neff.2022; @Engelhardt.2022; @Halsch.2021]. The rapidly increasing CTI, particularly at high elevations, suggests that cold-adapted species are being displaced by warm-adapted, low-elevation species. This phenomenon has been observed in the US Rocky Mountains where bumble bee communities are increasingly dominated by low-elevation species using high-elevation habitats as a thermal refugia [@Miller-Struttmann.2022]. An upslope range expansion appears to be a common response of

bumble bee communities to warming temperatures rather than expansions of northern ranges [@Kerr.2015; @Sirois-Delisle.2018]. Despite the rapid changes observed at higher latitudes, biological communities in southern latitudes and lower elevations are not protected from a changing climate [@Dillon.2010], and we documented some shifts in CTI in central Mexico and at low elevations. That said, if species lost from communities have STI values comparable to those species remaining, large shifts in CTI may be effectively masked, highlighting a limitation of our approach.

An increase in CTI could be the result of two mechanisms. First, shifts in the occurrence of bees within a community (i.e., immigration/extirpation of warm-/cool-adapted species via range expansion/contraction) and second, changes in the local abundance of warm-/cool-adapted species. We found evidence supporting both mechanisms by modeling occurrence and abundance-weighted measures of CTI. Shifts in local relative abundance align with existing research [@Hemberger.2021; @Cameron.2011]; however, substantial range expansion of warm-adapted bumble bees has not been described [@Kerr.2015] and may be unlikely given bumble bee dispersal capacities [@SiroisDelise.2018 but see @Fijen.2021]. That said, select species of bumble bees may be capable of long-distance dispersal [@Fijen.2021], and significant range shifts observed in other insect taxa have been observed [@Warren.2001; @Hinckling.2005]. Regardless, our jackknife analysis revealed that the largest contributors to increasing abundance and occurrence-based CTI within their range are common species that have exhibited both range increases [e.g., *B. impatiens* @Palmier.2019; @Looney.2019] and increases in local abundance. This result indicates that certain species are sensitive to and more capable of effectively tracking/adapting to ideal climatic conditions [@Maebe.2021]. The equivalent, northward spatial shift in bumble bee community composition that we observed was nearly identical to that of the spatial shift in maximum summer temperatures. This result provides further evidence that, at least some species, are successfully tracking warming climates and not accruing climate debts [@Devictor.2012]. However, other species (e.g., *B. occidentalis*) are not able to successfully track warming and are likely to suffer substantial reductions in range as a result [@Januosek.2023]. Such contrasts highlight the species-specific nature of bumble bee responses to a rapidly changing climate [@Jackson.2021; @Whitehorn.2021]. Additional research is needed detailing species-specific responses to warming conditions – focusing on identifying the physiological and evolutionary mechanisms that drive species' plasticity to changing environmental conditions.

An increase in the occurrence and abundance of warm adapted species does suggest a physiological/climate preference mechanism is at play (i.e., direct effect). Several studies document significant, direct effects of warming on insect pollinators [@Carradonna.2018; @Kenna.2021; @Hemberger.2022], however indirect effects mediated through biotic interactions may be just as if not more important [@Ockendon.2014]. In the context of our study, such indirect effects imply that shifts in bumble bee community composition are occurring in part in response to climate-induced changes in the resource landscape (i.e., indirect effects). For example, warming climates can widen the temporal availability of resources due to earlier snowmelts, which in turn lead to an increase in bumble bee abundance [@Ogilvie.2017]. Warming may also create phenological mismatches that reduce available forage for bees [@Pyke.2016, but see @Bartomeus.2011. Similarly, an

increase in hot, dry summer conditions can significantly reduce floral resources and the bumble bees that depend on them [@Iserbyt.2013], and similar patterns have been observed for butterflies [@Crossley.2021]. Unfavorable conditions, often a result of extreme weather events such as heat waves and droughts, can create resource bottlenecks that have the potential to lead to population declines and local extirpation [@Maron.2015]. Heat waves, for example, are expected to increase significantly in the coming century [@Meehl.2006; @Lopez.2018; @Thompson.2022]. As our study could not differentiate between direct and indirect pathways, parsing their relative impacts on bumble bees and other taxa is a critical research need. In the meantime, supporting bumble bees in the face of both direct and indirect effects may be accomplished by maintaining climate refugia, such as heterogeneity in vegetation structure, that can provide microclimatic respite from temperature extremes to bees [@Pincebourde.2020] and other taxa [e.g., birds, @Kim.2022] in addition to increasing spatial/temporal resource continuity to minimize negative indirect effects [@Maron.2015].

Given the spatiotemporal extent of our study, it is likely that warming summer temperatures and the temperature profile of a given bumble bee assemblage may co-vary with other, known factors of bumble bee community composition and occurrence. For example, losses in certain species across their range may be linked to disease [@Cameron.2011; @Colla.2006, @Szabo.2013]. Additionally, at large-scales, a loss of suitable habitat via land-use intensification and change is also of concern. However, when examined together with shifts in land-use, climatic variables (and their associated indirect effects) tend to have as much or more power to explain long-term species trends than land-use or resource availability in bumble [@Jackson.2021; @Kammerer.2020; @Whitehorn.2021, @Kerr.2015] and other wild bee species [@Duchenne.2020]. Moreover, the areas of greatest increase in CTI are in areas removed from the most significant effects of land-use change [e.g., high latitudes and elevations; @Halsch.2021]. Regardless, managing habitat offers a critical tool that can be used to mitigate the impacts of a changing climate [@Outhwaite.2022; @Oliver.2017; @Oliver.2015; @Kim.2022].

Conclusions

Climate change is poised to have significant, cross-scale impacts on insect behavior, populations, and communities [@Lehmann.2020; @Raven.2021; @Halsch.2021; @Høye.2021b]. In this paper, we document a substantial shift in the functional composition of bumble bee communities with respect to climate that is tied to a long-term increase of summer temperatures in North America. Due to changes in both occurrence and abundance, several species within bumble bee communities appear to be tracking climate warming, however this is likely at the expense of other species that lack the adaptive capacity to cope with rapidly climbing temperatures. Although the exact mechanisms of these community-level shifts remain unknown (i.e., direct vs. indirect effect of warming), our work adds to a growing body of evidence that suggests climate change will result in many climate losers with unknown consequences for ecosystems. It is critical that we focus on designing adaptation measures, such as climate refugia and climate-focused habitat conservation, to help combat the ongoing direct and indirect impacts a rapidly warming planet threatens. However, such efforts will only be successful in conjunction with

substantial decreases in emissions [@Oliver.2015] – an essential solution to safeguard the planet's biodiversity for generations to come.

Acknowledgements

Data access

All data and R code for analyses are available on FigShare via LINK (data) and LINK (code) and will be made public upon publication of this manuscript.

Figures and tables

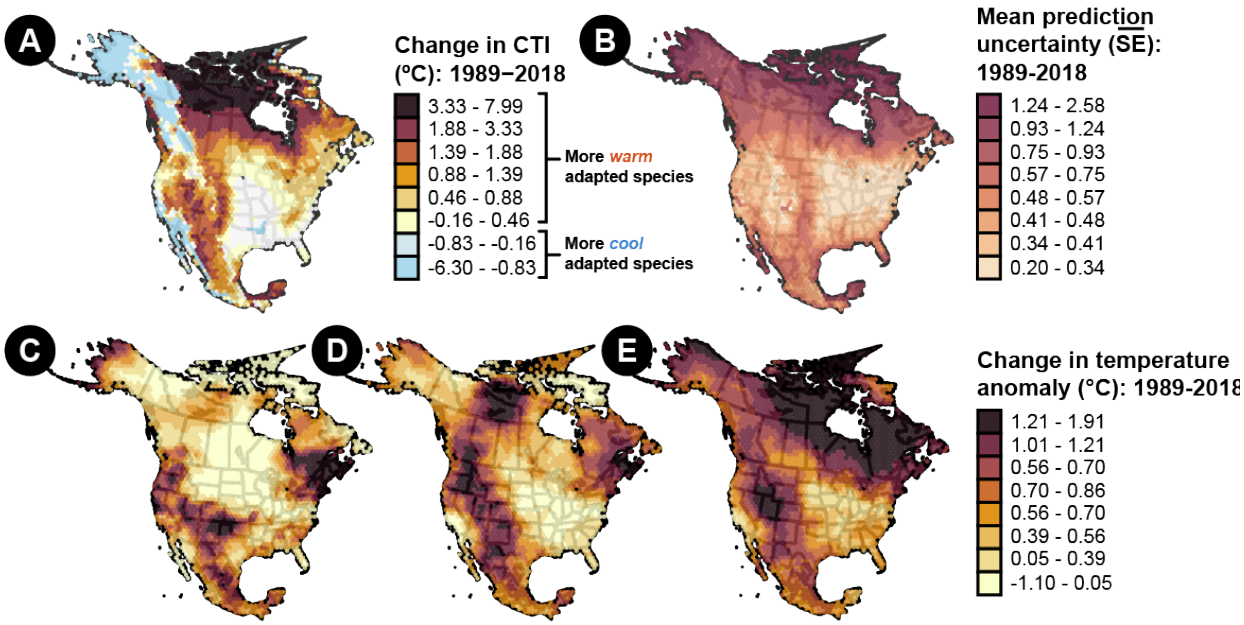

Figure 1: (A) Extrapolated spatial projection of the estimated change in community temperature index from 1990-2018 across North America. Differences in CTI were calculated for each grid cell by subtracting the model predicted $CTI_{t = 1989}$ from predicted $CTI_{t = 2018}$. (B) Spatial projection of the mean uncertainty estimates across years from 1989-2018. (C) Spatial projection of the change in the 3-year, 10-year (D) and 30-year (E) average temperature anomaly. Differences were calculated by subtracting the 1989 anomaly from the 2018 anomaly for each grid cell. Hexagonal grid cells are 100 km from side to side (~8600 km^2).

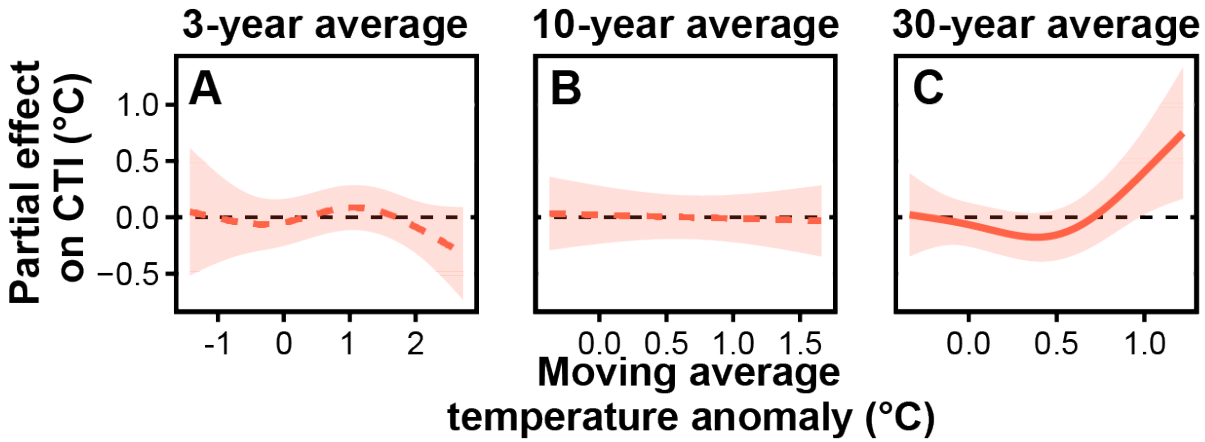

Figure 2: Generalized additive model partial plots (i.e., marginal effects) show the model predicted effect of (A) 3, (B) 10, and (C) 30-year moving average temperature anomalies on the community temperature index. Positive values on the x-axes indicate an increase in the average temperature relative to the long-term average. Solid line indicates significant trend.

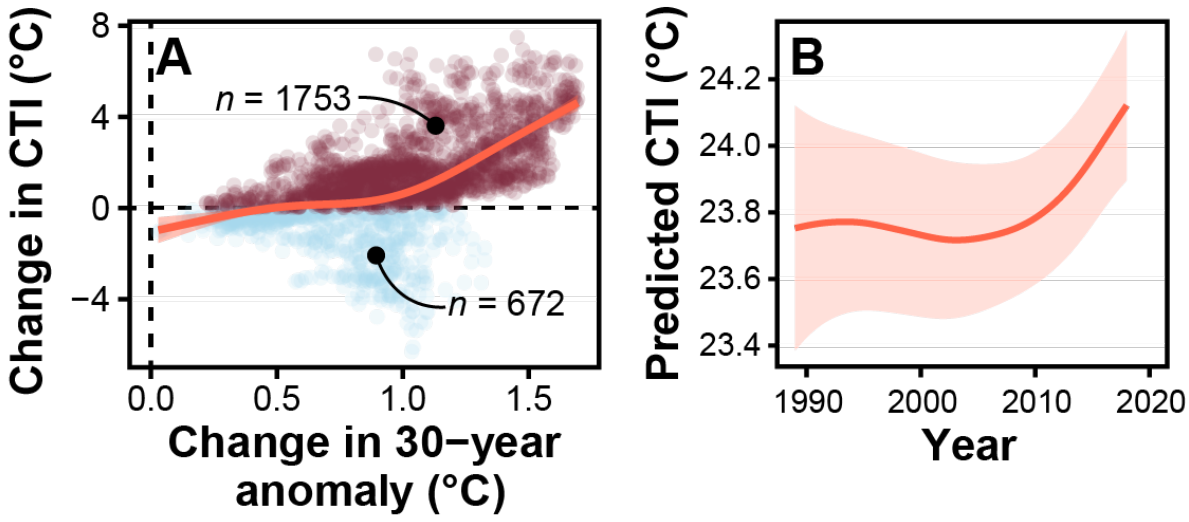

Figure 3: A significant increase in bumble bee CTI is strongly associated with long-term warming and has accelerated in the last 15 years. (A) Biplot of change in 30-year temperature anomaly and change in bumble bee CTI for each grid cell across North America. Trendline is a GAM fitted with ggplot and includes 95% confidence interval. Dashed lines indicate no change in anomaly or CTI for the X and Y axes, respectively. (B) Model estimated temporal trend in CTI across North America. Yearly predictions are calculated from the global model for each grid cell, and the trend within each region is illustrated with a GAM fit with 50% and 95% confidence intervals.

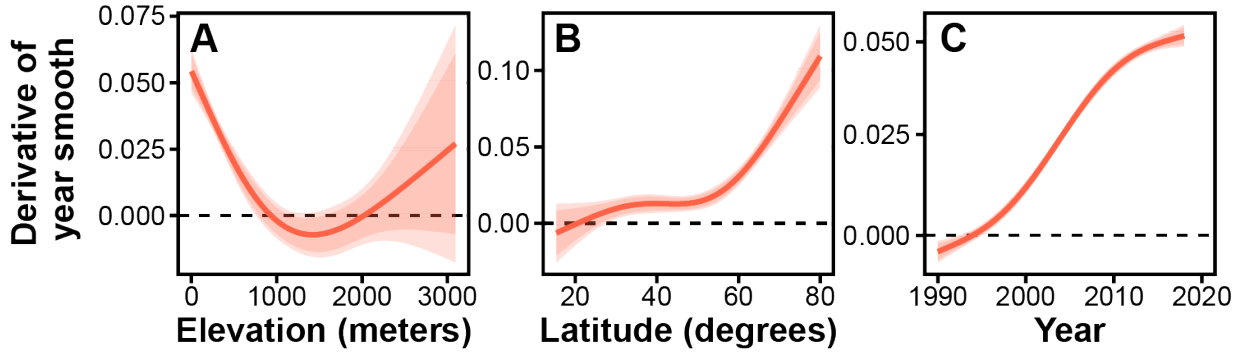

Figure 4: Estimates of the rate of change in CTI over time across (A) elevation, (B) latitude, and (C) year. Yearly predictions are calculated from the global model for each grid cell using simple generalized additive models with a single smooth of year to determine CTI trend within the grid cell. For each fitted smooth (except for the year, C), we then calculated the mean derivative across its range (1989-2018) for each grid cell. We then plotted these derivative estimates to explore, across the extent of North America, whether increases in CTI were varied with elevation or over time. We calculated predictions (red lines) from a generalized additive model using a thin-plate basis function and 3 knots for visual purposes only. Estimates include the 95% confidence interval.

References

Supplementary material

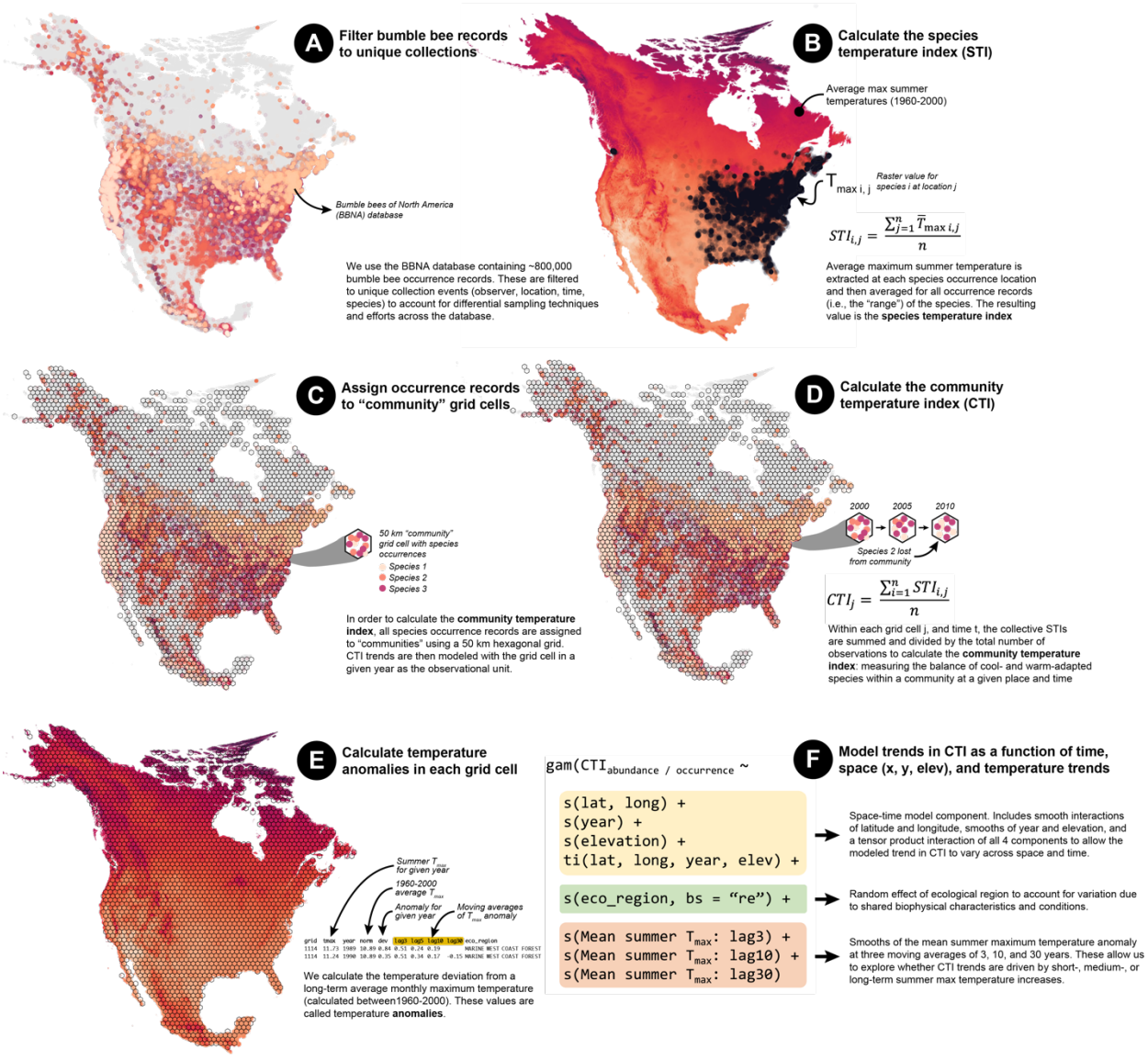

Figure S1: Conceptual figure of data cleaning (A), STI calculation (B), community assignment (C), CTI calculation (D), temperature anomaly calculations (E) and modeling procedures used in our analyses (F).

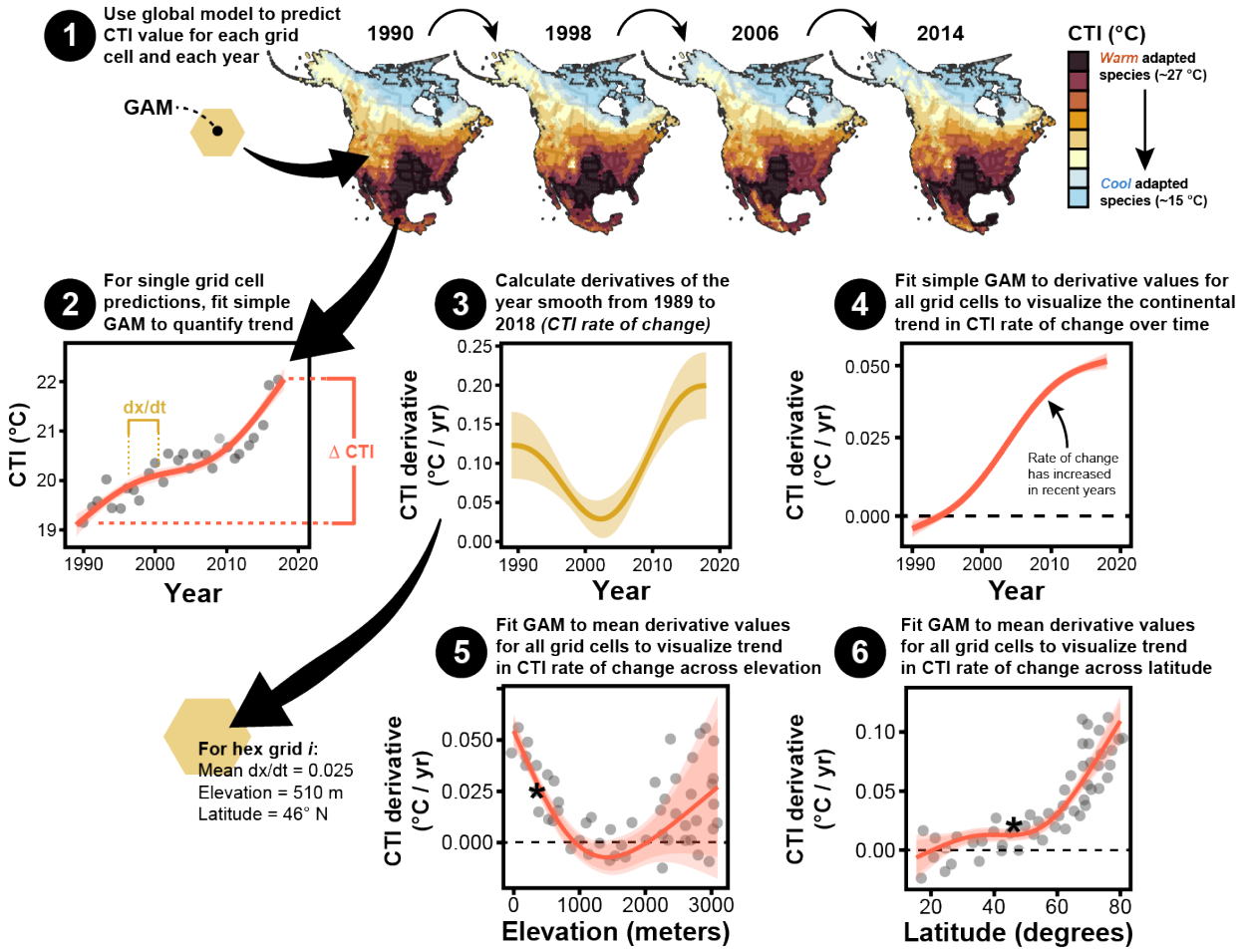

Figure S2: Conceptual diagram of the derivative calculations conducted to determine whether the rate of increase (i.e., derivative) of bumble bee CTI has remained steady or accelerated over space and time. (1) We use the global model to predict the CTI in each grid cell for each year of the study, from 1989-2018. (2) For each grid cell, we fit a GAM through the predicted points to visualize and quantify the trend in CTI from 1989-2018. From these data, we also calculated the change in CTI from 1989-2018 (Δ CTI) which is plotted in Fig. 1A. The overall change, however, tells us nothing of the functional form of the relationship between CTI and time, elevation, etc. To address this, we calculated the first derivative across the fitted smooth to determine how the rate of change in CTI varied across time, elevation, and latitude (Fig. 2). (3) For each grid cell's fitted GAM, we calculated the derivative of the year smooth at a range of values between 1989-2018. In this example, because CTI is increasing throughout the entire study period, the derivative is > 0 at all years. (4) We then took the derivative estimates for all grid cells and fit a GAM to visualize the trend between the derivative and time. For elevation (5) and latitude (6), we first averaged the derivative value from 1989-2018 to determine the mean slope for each grid cell before plotting that against the mean elevation and latitude of each grid cell and visualizing the relationship with a GAM. Transparent points are illustrative (not actual values) of individual hex grid derivative values across the range of elevation and latitude.

The black star represents a hypothetical mean derivative value from the example plot in (3) to illustrate how mean derivative values are used to assess the trend.

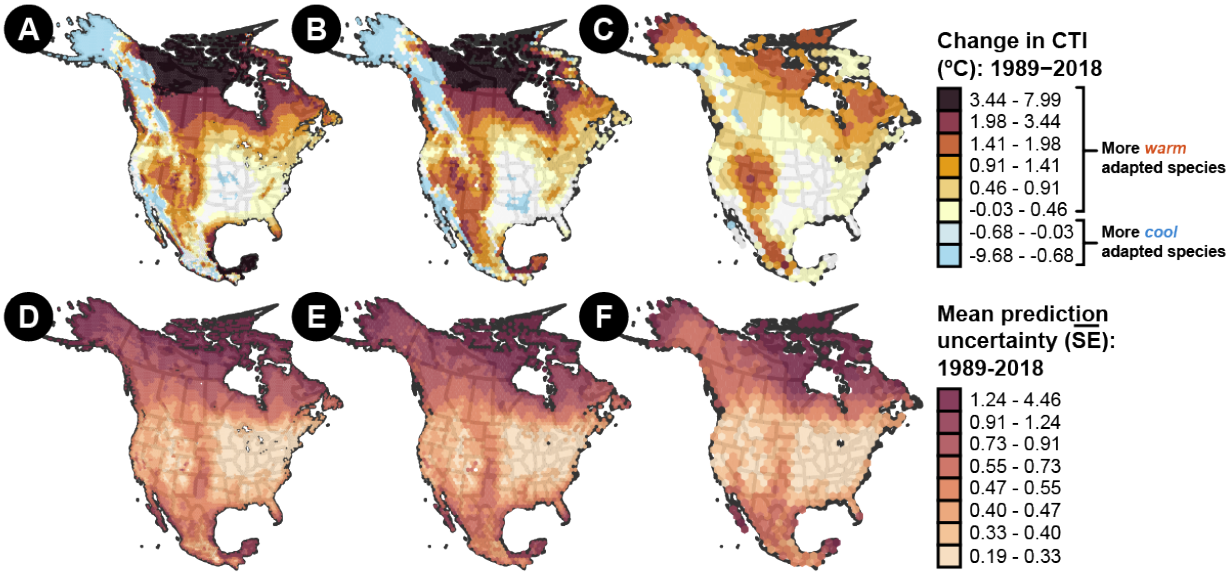

Figure S3: Predicted change in bumble bee CTI across North America between 1989-2018 at three different spatial resolutions of hexagonal grid (distance indicates side-to-side): (A) 50 km; (B) 100 km; (C) 200 km; along with the mean prediction uncertainty at the same resolutions.

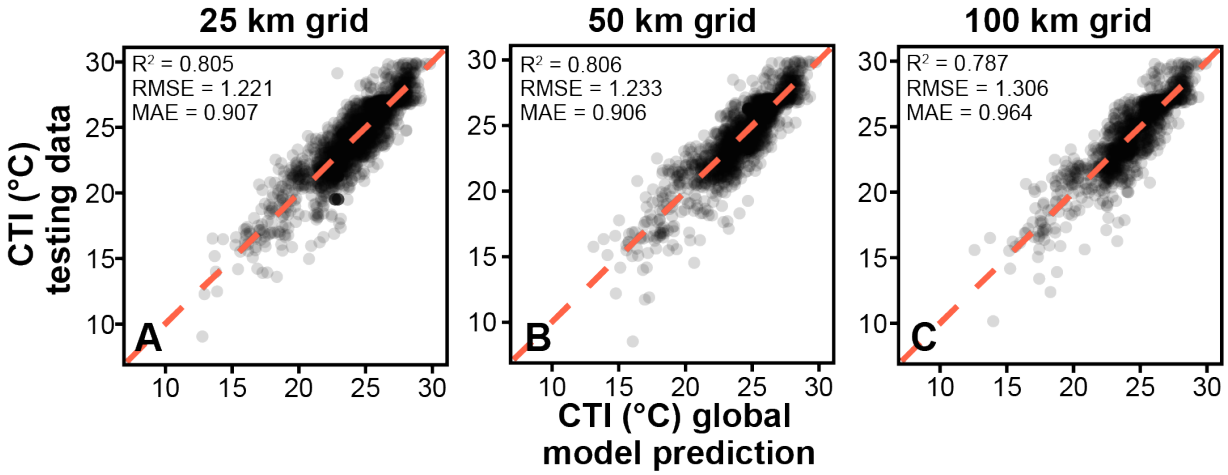

Figure S4: Abundance-weighted global model cross validation results at three different scales of (A) 25 km, (B) 50 km, and (C) 100 km center-to-edge hexagonal grids. Cross validation metrics are given in the top left of each panel including coefficient of determination (R^2), root mean squared error (RMSE), and mean absolute error (MAE).

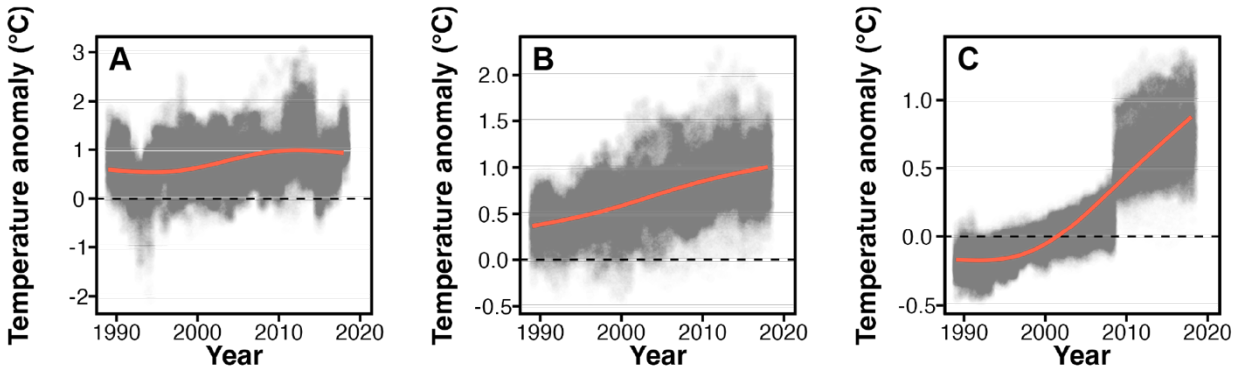

Figure S5: Trend in summer (June – September) maximum temperature anomalies at (A) 3-year, (B) 10-year, and (C) 30-year moving averages. Transparent points are raw values and red lines are GAM trendlines.

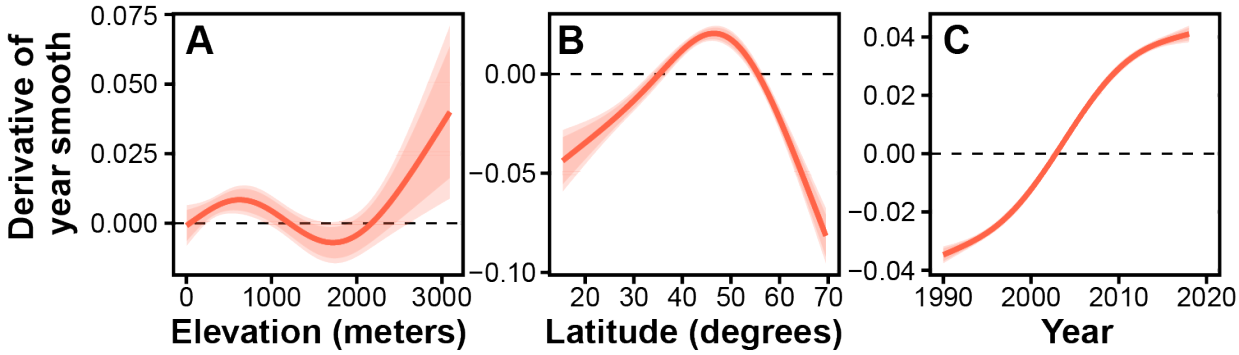

Figure S6: Estimates of the rate of change in CTI over time across (A) elevation, (B) latitude, and (C) year using predictions only from grid cells containing occurrence records (conservative approach). Yearly predictions are calculated from the global model for each grid cell using simple generalized additive models with a single smooth of year to determine CTI trend within the grid cell. For each fitted smooth (except for the year, C), we then calculated the mean derivative across its range (1989-2018) for each grid cell. We then plotted these derivative estimates to explore, across the extent of North America, whether increases in CTI were varied with elevation or over time. We calculated predictions (red lines) from a generalized additive model using a thin-plate basis function and 3 knots for visual purposes only. Estimates include the 95% confidence interval.

Table S1: Results from a generalized additive model for CTI using occurrence-only and abundance-weighted records from 1989-2018.

	Occurrence model			Abundance model		
Model smooth	**EDF**	**F**	**p value**	**EDF**	**F**	**p value**
Latitude, longitude	282.065	16.778	< 0.001	270.546	18.099	< 0.001
Year	2.945	4.015	0.004	2.353	3.592	0.022
Elevation	7.995	23.926	< 0.001	7.615	25.782	< 0.001
Latitude, longitude, elevation, year	100.149	3.782	< 0.001	97.853	2.996	< 0.001
Ecological region	10.526	2.388	< 0.001	9.855	1.644	< 0.001
Mean Tmax 3-year MA	2.968	2.584	0.032	2.827	2.500	0.039
Mean Tmax 10-year MA	1.002	0.064	0.803	1.001	0.475	0.491
Mean Tmax 30-year MA	2.967	4.561	0.002	3.377	6.712	< 0.001
Model n	5273			5273		
Deviance explained	0.860			0.863		
R-squared (adjusted)	0.849			0.851		

*EDF :estimated degrees of freedom (i.e., smooth wiggliness)

Table S2: Results from a generalized additive model for CTI using occurrence-only records at three different spatial resolutions (community grid scale) at 25, 50, and 100 km from 1989-2018.

	25 km grid scale			50 km grid scale			100 km grid scale		
Model smooth	**EDF**	**F**	**p value**	**EDF**	**F**	**p value**	**EDF**	**F**	**p value**
Latitude, longitude	294.224	18.839	< 0.001	270.546	18.099	< 0.001	181.650	17.769	< 0.001
Year	3.653	5.293	< 0.001	2.353	3.592	0.022	2.538	1.609	0.164
Elevation	9.360	34.646	< 0.001	7.615	25.782	< 0.001	1.000	52.860	< 0.001
Latitude, longitude, elevation, year	106.844	4.744	< 0.001	97.853	2.996	< 0.001	51.223	2.558	< 0.001
Ecological region	10.889	4.824	< 0.001	9.855	1.644	< 0.001	11.650	4.843	< 0.001
Mean Tmax 3-year MA	2.881	3.999	0.008	2.827	2.500	0.039	1.000	0.041	0.840
Mean Tmax 10-year MA	1.000	0.061	0.805	1.001	0.475	0.491	3.511	5.344	0.004
Mean Tmax 30-year MA	2.919	5.177	0.001	3.377	6.712	< 0.001	3.029	4.430	0.003
Model n	7582			5273			3078		
Deviance explained	0.840			0.860			0.862		
R-squared (adjusted)	0.831			0.849			0.850		

*EDF :estimated degrees of freedom (i.e., smooth wiggliness)

Table S3: Jackknife analysis for both abundance-weighted and occurrence CTI estimates for all species in the dataset. Species temperature index (STI), STI standard deviation, and number of records in the CTI dataset are also given. Percent difference is the difference between the global (including all species) and jackknife model (excluding single species) mean derivative $\left(\frac{dx}{dt}\right)$ across the temporal range (1989-2018) of the respective global model. Positive percentages indicate that the species contributes to the CTI trend (i.e., that an increase in abundance/occurrence leads to an increase in CTI).

MOST REPRESENTED SPECIES ***(n records > 1000)***

Species	Subgenus	IUCN redlist category	STI	STI S.D.	Number of records	Global *dx/dt* (abundance)	Global *dx/dt* (occurrence)	Jackknife *dx/dt* (abundance)	Jackknife *dx/dt* (occurrence)	% difference (abundance)	% difference (occurrence)
B. occidentalis	Bombus	Vulnerable	21.688	4.862	2357	0.018	0.018	0.005	0.002	70.424	89.202
B. nevadensis	Bombias	Least Concern	24.539	4.102	2236	0.018	0.015	0.005	0.003	69.653	81.752
B. ephippiatus	Pyrobombus	Least Concern	23.715	3.426	3153	0.023	0.021	0.008	0.005	66.868	75.315
B. bifarius	Pyrobombus	Least Concern	22.023	4.132	3237	0.024	0.023	0.008	0.007	66.716	69.324
B. vosnesenskii	Pyrobombus	Least Concern	25.585	4.016	7514	0.025	0.021	0.009	0.008	64.318	63.772
B. huntii	Pyrobombus	Least Concern	25.764	3.066	4556	0.019	0.016	0.007	0.004	64.161	72.12
B. impatiens	Pyrobombus	Least Concern	27.019	2.507	52373	0.021	0.015	0.008	0.005	62.382	63.191
B. appositus	Subterraneobombus	Least Concern	22.644	3.263	1204	0.03	0.024	0.013	0.009	55.057	60.367
B. centralis	Pyrobombus	Least Concern	23.806	3.602	1991	0.016	0.014	0.008	0.006	50.166	58.733
B. pensylvanicus	Thoracobombus	Vulnerable	29.817	3.057	16763	0.019	0.012	0.01	0.006	44.172	51.223
B. flavifrons	Pyrobombus	Least Concern	20.427	4.126	3274	0.03	0.028	0.018	0.015	40.272	44.577
B. griseocollis	Cullumanobombus	Least Concern	27.017	2.306	21310	0.033	0.027	0.02	0.014	38.469	47.951
B. sylvicola	Pyrobombus	Least Concern	17.018	4.312	1093	0.049	0.044	0.031	0.028	35.224	37.181
B. auricomus	Bombias	Least Concern	27.586	1.834	3172	0.018	0.012	0.012	0.007	35.221	40.898
B. insularis	Psithyrus	Least Concern	22.194	3.755	1415	0.026	0.022	0.017	0.013	34.774	40.71
B. melanopygus	Pyrobombus	Least Concern	22.486	5.575	5054	0.036	0.031	0.023	0.019	34.355	36.794
B. bimaculatus	Pyrobombus	Least Concern	26.563	2.086	13788	0.016	0.009	0.01	0.005	33.454	40.704
B. fervidus	Thoracobombus	Vulnerable	25.637	2.887	7192	0.027	0.022	0.018	0.013	32.296	39.02
B. frigidus	Pyrobombus	Least Concern	16.409	5.531	1043	0.042	0.038	0.028	0.024	32.164	36.044
B. terricola	Bombus	Vulnerable	22.795	1.987	3905	0.038	0.032	0.026	0.021	31.586	34.711
B. flavidus	Psithyrus	Data Deficient	20.051	2.875	1242	0.039	0.034	0.029	0.025	25.842	27.554
B. perplexus	Pyrobombus	Least Concern	23.724	2.571	4428	0.043	0.037	0.032	0.026	25.713	29.98
B. rufocinctus	Cullumanobombus	Least Concern	23.628	2.739	5306	0.028	0.023	0.022	0.017	24.284	27.606
B. vagans	Pyrobombus	Least Concern	24.615	2.401	7713	0.027	0.021	0.022	0.017	18.602	20.168
B. mixtus	Pyrobombus	Least Concern	20.269	5.038	3628	0.044	0.04	0.037	0.031	16.611	22.522
B. borealis	Subterraneobombus	Least Concern	22.960	1.999	3355	0.033	0.028	0.031	0.026	7.942	8.631
B. citrinus	Psithyrus	Least Concern	25.139	2.138	2229	0.032	0.024	0.031	0.023	2.711	1.935
B. affinis	Bombus	Critically Endangered	25.511	1.710	2188	0.016	0.007	0.016	0.009	-4.755	-24.531
B. ternarius	Pyrobombus	Least Concern	22.954	1.731	10215	0.036	0.03	0.039	0.03	-7.966	-1.741

LESS REPRESENTED SPECIES ***(n records < 1000)***

Species	Subgenus	IUCN redlist category	STI	STI S.D.	Number of records	Global *dx/dt* (abundance)	Global *dx/dt* (occurrence)	Jackknife *dx/dt* (abundance)	Jackknife *dx/dt* (occurrence)	% difference (abundance)	% difference (occurrence)
B. macgregori	Cullumanobombus	Least Concern	22.475	0.000	71	0	0.003	0.001	-0.007	1781.842	331.519
B. trinominatus	Thoracobombus	Least Concern	16.550	0.328	223	0.005	0.005	-0.004	-0.005	180.522	196.414
B. steindachneri	Thoracobombus	Endangered	28.613	3.072	321	0.016	0.017	-0.003	-0.002	118.408	110.735
B. haueri	Cullumanobombus	Endangered	22.698	3.456	45	0.024	0.024	-0.001	-0.001	104.39	104.082
B. brachycephalus	Cullumanobombus	Endangered	25.308	1.878	96	0.015	0.013	0	-0.001	102.073	110.963
B. weisi	Thoracobombus	Least Concern	22.650	2.167	994	0.016	0.015	0.001	0	95.591	97.538
B. mexicanus	Thoracobombus	Vulnerable	29.125	3.111	94	0.016	0.013	0.001	-0.001	91.596	107.946
B. diligens	Thoracobombus	Near Threatened	26.415	2.185	334	0.023	0.02	0.002	0.002	91.55	91.555
B. jonellus	Pyrobombus	Data Deficient	16.233	2.632	359	0.028	0.033	0.006	0.009	78.321	74.001
B. caliginosus	Pyrobombus	Vulnerable	23.542	3.050	282	0.014	0.008	0.003	0	78.248	102.669
B. fraternus	Cullumanobombus	Endangered	30.611	2.308	927	0.007	0.002	0.002	-0.001	78.176	172.649
B. medius	Thoracobombus	Vulnerable	28.500	2.486	609	0.029	0.021	0.009	0.004	70.17	82.763
B. vandykei	Pyrobombus	Least Concern	27.423	4.228	464	0.018	0.012	0.006	0.002	69.842	87.082
B. cryptarum	Bombus	Data Deficient	7.373	6.161	779	0.028	0.032	0.008	0.008	69.7	75.074
B. neoboreus	Alpinobombus	Data Deficient	7.884	6.184	43	0.056	0.056	0.022	0.022	61.607	61.048
B. variabilis	Psithyrus	Critically Endangered	29.661	2.587	92	0.017	0.01	0.007	0.003	59.301	73.525
B. franklini	Bombus	Critically Endangered	25.076	4.501	64	0.012	0.005	0.006	0.002	53.69	55.804
B. kirbiellus	Alpinobombus	Data Deficient	14.843	5.930	280	0.039	0.038	0.023	0.02	42.119	45.946
B. polaris	Alpinobombus	Data Deficient	9.753	5.012	96	0.06	0.057	0.038	0.032	36.908	43.165
B. natvigi	Alpinobombus	Data Deficient	7.473	5.901	16	0.075	0.071	0.048	0.038	35.874	46.663
B. morrisoni	Cullumanobombus	Vulnerable	27.991	3.534	489	0.035	0.028	0.024	0.019	30.837	31.588
B. pullatus	Thoracobombus	Data Deficient	30.905	0.253	41	0.039	0.023	0.028	0.021	27.867	8.659
B. suckleyi	Psithyrus	Critically Endangered	22.644	3.220	86	0.048	0.042	0.036	0.03	24.935	28.31
B. bohemicus	Psithyrus	Data Deficient	22.839	2.339	320	0.043	0.038	0.033	0.028	23.413	27.549
B. sandersoni	Pyrobombus	Least Concern	22.221	2.361	765	0.044	0.037	0.038	0.031	13.727	14.44
B. sitkensis	Pyrobombus	Least Concern	21.060	3.909	534	-0.005	-0.003	-0.007	-0.006	-27.155	-124.088